

The Scaling of Broadband Shock-Associated Noise with Increasing Temperature

Steven A. E. Miller*

The National Aeronautics and Space Administration

Abstract

A physical explanation for the saturation of broadband shock-associated noise (BBSAN) intensity with increasing jet stagnation temperature has eluded investigators. An explanation is proposed for this phenomenon with the use of an acoustic analogy. To isolate the relevant physics, the scaling of BBSAN peak intensity level at the sideline observer location is examined. The equivalent source within the framework of an acoustic analogy for BBSAN is based on local field quantities at shock wave – shear layer interactions. Propagation of sound through the jet shear layer is predicted with an adjoint vector Green’s function solver of the linearized Euler equations. The combination of the equivalent source and adjoint vector Green’s function allows for correct predictions of the saturation of BBSAN with increasing stagnation pressure and stagnation temperature. The sources and vector Green’s function have arguments involving the steady Reynolds-Averaged Navier-Stokes solution of the jet. It is proposed that saturation of BBSAN with increasing jet temperature occurs due to a balance between the amplification of the sound propagation through the shear layer and the source term scaling.

*Research Aerospace Engineer, Aeroacoustics Branch, NASA Langley Research Center, 2 N. Dryden St. MS 461, Hampton, VA, 23681, USA, s.miller@nasa.gov

Personal Introduction

It is a privilege to contribute an article to this special edition in honor of Dr. Fereidoun ‘Feri’ Farassat. The present article involves the use of an acoustic analogy and a Green’s function for its solution. Dr. Farassat’s career was heavily involved with both of these fundamental methods in aeroacoustics since his Ph.D. [1] work at Cornell (under advisement of Professor William R. Sears) based on the work of J. E. Ffowcs Williams and D. L. Hawkings [2]. His Ph.D. work laid the foundation for the rest of his career at NASA Langley Research Center (LaRC) within the Aeroacoustics Branch. Dr. Farassat’s developments such as Formulation 1 (Farassat [3]), Formulation 1A (Farassat and Succi [4]), the use of generalized functions (Farassat and Myers [5]), and countless others, were extremely important for the field. Some of these contributions are available on the NASA Technical Reports Server, where Dr. Farassat has over 130 publications available to the public on a wide range of topics.

Dr. Farassat, during his mid- to late-career, was undoubtedly the theoretical backbone of the Aeroacoustics Branch at NASA Langley. He had influenced the technical direction of many researchers within both the branch and NASA as a whole, and had a considerable influence throughout the community, all of which are still being felt today.

Dr. Farassat had a long history of imparting his knowledge to new researchers at NASA Langley. Some of my first and most memorable interactions with Dr. Farassat had started with these teachings. I enjoyed many technical discussions in his office and his guidance changed my technical viewpoint, especially relating to the acoustic analogy. These discussions saved me large amounts of time and helped me avoid many possible technical failures. He also was not afraid to offer advice, technical or personal, and was genuinely interested in the well-being of everyone he interacted with. He was an unwavering advocate within NASA for the importance of research and was extremely supportive of junior researchers.

I am proud to call Dr. Farassat my colleague and friend. Thank you Feri for the time we had together.

1 Introduction

Unfortunately, there is no first principles mathematical model or physical understanding of how broadband shock-associated noise (BBSAN) scales with increasing stagnation temperature. This paper attempts to examine the scaling of BBSAN intensity with increasing stagnation temperature via the acoustic analogy of Morris and Miller [6]. This is accomplished by examining the peak intensity at the sideline location relative to the jet centerline axis. The equivalent source of the BBSAN is modeled with the use of local instead of ambient quantities of a steady Reynolds-Averaged Navier-Stokes (RANS) solution of the jet exhaust and a simple model of the two-point velocity cross-correlation. Noise propagation is accurately modeled by using an adjoint vector Green’s function solver for the linearized Euler equations (LEE). The scaling is compared with the measurements of Kuo *et al.* [7] for a design Mach number $M_d = 1.50$ nozzle at over- and under-expanded conditions, and with the measurements of Bridges and Brown [8] for a convergent nozzle. Comparisons cover the range of total temperature ratios (TTR) from one to four. The equivalent source model combined with accurate calculations of the propagation of BBSAN through the jet shear layer allows for predictions that retain the scaling with respect to nozzle pressure ratio (NPR) and allows for the saturation of BBSAN with increasing TTR.

Jet noise is due to multiple unique sources. Lossless noise spectra from an off-design singlestream supersonic jet can be observed in the far-field as shown in Fig. 1. The x -axis represents non-dimensional frequency as Strouhal number, St , which is frequency normalized by the fully expanded jet velocity, u_j , and the fully expanded jet diameter, D_j . The fully expanded diameter is the equivalent nozzle exit diameter that produces an on-design flow. The y -axis represents the Sound Pressure Level (SPL) per unit St referenced to twenty micro Pascals. The observer angle ψ is measured from the upstream axis of the jet centerline to the observer in the far-field about the nozzle exit plane. The non-dimensional distance from the nozzle exit to the observer is $R/D = 100$, where R is the distance and D is the nozzle diameter.

Shock-associated noise consists of discrete tones often called ‘screech,’ first observed and described by Powell [9]; and BBSAN was first extensively modeled and studied by Harper-Bourne and Fisher [10]. Screech (see Raman [11] for an overview) has a large effect on BBSAN which will be illustrated below. BBSAN results when large-scale coherent turbulent structures interact with the shock waves in the jet shear layer. Each interaction of turbulence with in-

dividual oblique shock waves represents a source that contributes to BBSAN. The noise combines constructively or destructively in the far-field to produce the broad humps that are seen in Fig. 1. BBSAN is less intense in the downstream direction than mixing noise due to refraction effects. In the sideline and upstream directions ($\psi = 90$ and $\psi = 50$ deg. in Fig. 1 respectively) BBSAN dominates the mixing noise over a wide range of frequencies. The peak frequency of BBSAN varies with observer angle and jet operating conditions. For overviews of jet noise consult Ffowcs Williams [12], Ffowcs Williams [13], or Goldstein [14]; and specifically for supersonic jet noise consult Tam [15].

The question arises regarding how BBSAN scales with increasing temperature. The scaling of BBSAN with increasing TTR can be observed experimentally in Fig. 2. The trend is similar (in terms of intensity scaling and ‘saturation’) across observer angles, jet Mach numbers, and nozzle geometries. The phenomenon is summarized excellently by Viswanathan *et al.* [16] who state, “The levels increase as the jet is first heated; however, the levels do not increase with further increase in jet temperature. The physical phenomenon responsible for this saturation of levels is not known at this time.”

Harper-Bourne and Fisher [10] observed that the intensity of BBSAN is proportional to the fourth power of an off-design parameter, β . This parameter was defined by Harper-Bourne and Fisher for convergent nozzles and is extended to the general case as,

$$\beta = \sqrt{|M_j^2 - M_d^2|}, \quad (1)$$

where M_d is the nozzle design Mach number, which is dependent on the ratio of the exit area to the throat area, and M_j is the fully expanded Mach number, which is only dependent on the NPR and the ratio of specific heats γ . It was shown this trend holds over a wide range of fully expanded Mach numbers for a wide range of convergent and convergent-divergent nozzles. Note that the 4th power of β may vary slightly due to small effects of heating and sound emission angle (see Viswanathan *et al.* [16] for details). At higher β the relationship is no longer linear and the slope of β^4 versus NPR drops off slightly. Equation 1 is relatively independent of TTR.

Harper-Bourne and Fisher [10] write, “... the intensity of shock noise is a function only of pressure ratio, and is independent of jet stagnation temperature and hence jet efflux velocity.” This statement is in the context of a larger study and conflicts with more recent experimental observations. In

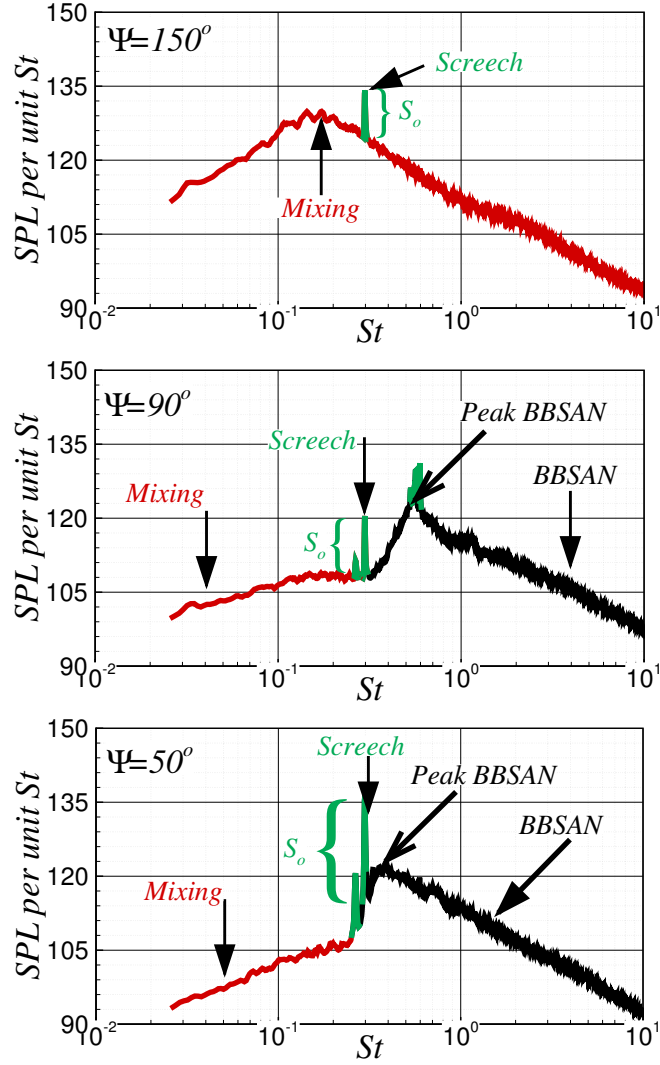


Figure 1: Lossless sound pressure level per unit Strouhal number at $R/D = 100$ resulting from a $M_d = 1.00$, $M_j = 1.50$, and TTR = 1.00 jet. ψ is the angle from the upstream jet axis to the observer centered about the nozzle exit. S_o is the screech over-pressure.

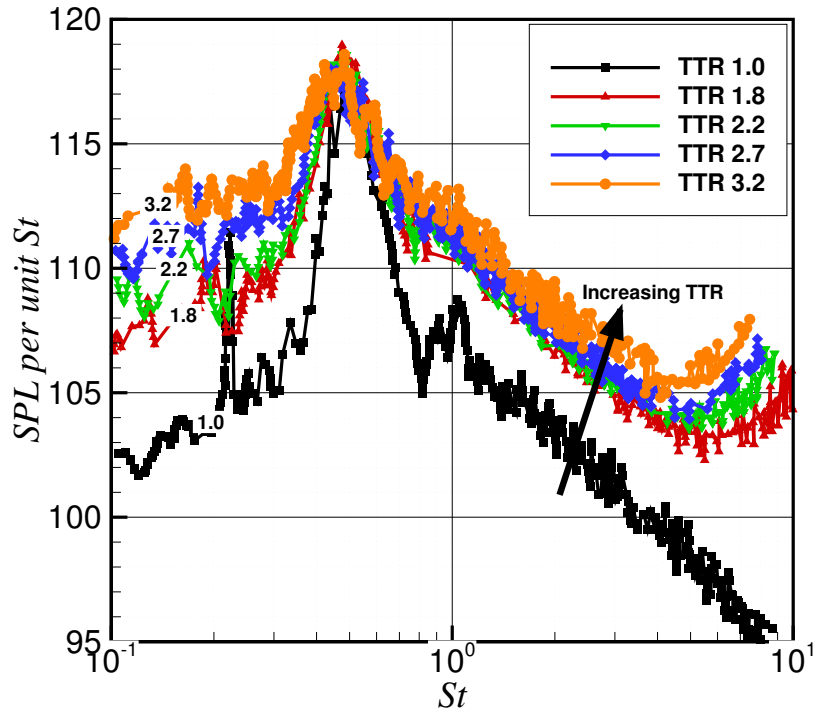


Figure 2: Lossless spectra for a $M_j = 1.71$ and $D = 0.06223$ m jet at $R/D = 97.86$ and $\psi = 90$ degrees. The spectra corresponds to a TTR of 1.00, 1.80, 2.20, 2.70, and 3.20. This figure is reproduced from Viswanathan *et al.* [16] with permission.

the experiments of Viswanathan [16] and Kuo *et al.* [7] there are noticeable differences in BBSAN intensity when holding NPR constant and varying TTR. These differences are often unnoticeable if the jet is non-screeching (when the jet is heated) compared to a jet that is screeching (when the jet is cold), which is often the case in small laboratory experiments. This is due to the very large effect that screech tones have on BBSAN (see Andre *et al.* [17] for details). It is important to isolate the scaling of BBSAN intensity from the varying NPR and from the effect of various screech intensities, which are a function of NPR and TTR.

Tam [18] developed a method for BBSAN prediction and the basic physical model is described by Tam and Tanna [19]. Tam argued that the shock cell structure in the jet could be modeled, following the work of Pack [20]. The large-scale turbulence in the jet shear layer is modeled as a random superposition of instability waves supported by the jet mean flow, as described by Tam and Chen [21]. Tam [22] modified the model by Tam [18] to include the capability to predict BBSAN from heated jets up to a moderate off-design parameter, β . A temperature correction factor, T_{cf} , was included to correct for the over-prediction at all frequencies due to increasing TTR. Tam used the following empirical correction factor for heated jet predictions,

$$T_{cf} = \frac{\rho_j}{\rho_\infty} \left(1 + \frac{\gamma - 1}{2} M_j^2 \right)^{-1}, \quad (2)$$

where ρ_j is the fully expanded density, ρ_∞ is the ambient static density, and γ is the ratio of specific heats. Morris and Miller [6] formed an acoustic analogy for BBSAN and later showed its application to a wide variety of fully expanded Mach numbers and temperature ratios, for cylindrical, dual-stream, and rectangular nozzles, with over- and under-expanded jet plumes. To account for the slight heating effects on the predicted BBSAN relative to experimental data, Eqn. 2 was used to scale the spectral density.

Recently, Kuo *et al.* [7] performed experiments that examined the effects of heating on BBSAN in the far-field by examining three nozzle geometries. The first was convergent and the others were convergent-divergent at $M_d = 1.50$ and $M_d = 1.76$. The effects of jet flow heating were simulated with a helium-air mixture. Doty and McLaughlin [23] had shown that helium-air jets and heated jets have similar physical and acoustic properties in the far-field. Kuo *et al.* [7] examined heating effects for the $M_d = 1.50$ nozzle at $M_j = 1.2, 1.4, 1.7,$ and 1.9 by varying TTR from 1.0 to 2.2. In the

following sections, a scaling relationship is developed for BBSAN intensity with increasing TTR, and the relationship is compared with measurement for four cases. The arguments of the scaling relationship are based upon steady RANS solutions and details of the calculations are shown.

2 Mathematical Analysis

The Euler equations are rearranged into a linear left hand side operator of the LEE and right hand side equivalent sources. The equivalent source of the continuity equation is the dilatation and the equivalent source of the momentum equation is the unsteady force per unit volume involving velocity fluctuations of the shocks and turbulence in the jet plume. The latter is of interest for BBSAN prediction. The acoustic pressure is found from the convolution integral of the vector Green's function with the equivalent sources. The spectral density is then formulated by the Fourier transform of the autocorrelation involving acoustic pressure. The full details of this approach are shown in Morris and Miller [6] and result in,

$$S(\mathbf{x}, \omega) = \rho_\infty^2 c_\infty^4 \int_{-\infty}^{\infty} \dots \int_{-\infty}^{\infty} \sum_{n=1}^3 \sum_{m=1}^3 \pi_g^{n*}(\mathbf{x}, \mathbf{y}, \omega) \pi_g^m(\mathbf{x}, \mathbf{y} + \boldsymbol{\eta}, \omega) \times R_{nm}^v(\mathbf{y}, \boldsymbol{\eta}, \tau) \exp[-i\omega\tau] d\tau d\boldsymbol{\eta} d\mathbf{y}, \quad (3)$$

where S is the spectral density, c is the speed of sound, π_g^n is the n^{th} component of the vector Green's function of the LEE, $R_{mn}^v(\mathbf{y}, \boldsymbol{\eta}, \tau)$ is the two-point cross-correlation of the equivalent source, \mathbf{x} is a vector from the nozzle exit to the observer, and \mathbf{y} is a vector from the nozzle exit to a source in the jet. $\boldsymbol{\eta} = \boldsymbol{\eta}(\xi, \eta, \zeta)$ is a vector between two spatial locations in the jet source region.

The vector Green's function of the LEE as shown in Eqn. 3 is defined by the solution of,

$$\frac{D_o \pi_g^n}{Dt} + \frac{\partial u_{gi}^n}{\partial x_i} = \delta(\mathbf{x} - \mathbf{y}) \delta(t - \tau) \delta_{0n}, \quad (4)$$

and,

$$\frac{D_o u_{gi}^n}{Dt} + u_{gj} \frac{\partial \bar{u}_i}{\partial x_j} + \bar{c}^2 \frac{\partial \pi_g^n}{\partial x_i} = \delta(\mathbf{x} - \mathbf{y}) \delta(t - \tau) \delta_{in}, \quad (5)$$

where D_o is the material derivative about the meanflow and u is the velocity. The vector Green's function is periodic and has the identity $\pi_g^{n*}(\mathbf{x}, \mathbf{y}, \omega) = \pi_g^n(\mathbf{x}, \mathbf{y}, -\omega)$. General analytic solutions of Eqns. 4 and 5 are unknown. However, numerical solutions can be found that are related to Lilley's [24] equation. Strategies to find highly accurate numerical solutions of the vector Green's function are discussed in Tam and Auriault [25], Raizada [26], and Khavaran *et al.* [27]. Propagation effects have been examined for BBSAN using these techniques by Miller and Morris [28] and a ray method by Henry *et al.* [29]. The approach of Miller and Morris is employed here to find π_g^n . R_{nm}^v takes the form,

$$R_{nm}^v(\mathbf{y}, \boldsymbol{\eta}, \tau) = \overline{f_n^v(\mathbf{y}, t) f_m^v(\mathbf{y} + \boldsymbol{\eta}, t + \tau)}, \quad (6)$$

where f_i^v is the equivalent source involving second order fluctuations of the momentum term in the governing equations, which is defined as,

$$f_i^v = -u_{sj} \frac{\partial u_{ti}}{\partial x_j} - u_{tj} \frac{\partial u_{si}}{\partial x_j}, \quad (7)$$

where \mathbf{u} are velocity fluctuations associated with the shocks, s , and the turbulence, t , and x_i are independent spatial coordinates. In Morris and Miller [6] the equivalent source is formulated based on dimensional and physical arguments involving the speed of sound, c , the integral turbulent length scale in the streamwise direction, l , the pressure due to the shock waves, p_s , and the density, ρ . In this work, the density, speed of sound, and streamwise velocity component are local instead of ambient values. The density and speed of sound at the shock wave – shear layer interactions are arguments of the source model, and are dependent upon the local static temperature. A model for $\overline{f_n^v(\mathbf{y}, t) f_m^v(\mathbf{y} + \boldsymbol{\eta}, t + \tau)}$ is formed,

$$\overline{f_n^v(\mathbf{y}, t) f_m^v(\mathbf{y} + \boldsymbol{\eta}, t + \tau)} = \frac{p_s(\mathbf{y}) p_s(\mathbf{y} + \boldsymbol{\eta})}{\rho^2 c^2 l^2} R(\mathbf{y}, \boldsymbol{\eta}, \tau), \quad (8)$$

where $R(\mathbf{y}, \boldsymbol{\eta}, \tau)$ is the two-point cross-correlation of the velocity fluctuations. Assume that the time and spatial terms of $R(\boldsymbol{\eta}, \tau)$ are separable as Ribner [30] postulated and model the two point cross-correlation of the fluctuating turbulent velocity as,

$$R(\mathbf{y}, \boldsymbol{\eta}, \tau) = a_{mn} K(\mathbf{y}) \exp[-\tau^2/\tau_s^2] \exp[-(\xi - u_c \tau)^2/l^2] \times \exp[-(\eta^2 + \zeta^2)/l_\perp^2], \quad (9)$$

where a_{mn} are coefficients that can be set for anisotropic turbulence, l_{\perp} is the cross-stream length scale, K is the turbulent kinetic energy, u_c is the streamwise convection velocity, and ξ , η , and ζ are components of the vector $\boldsymbol{\eta}$.

Substituting Eqns. 8 and 9 into Eqn. 3 and isolating the integral involving τ yields,

$$\int_{-\infty}^{\infty} \exp[-i\omega\tau] \exp[-\tau^2/\tau_s^2] \exp[-(\xi - u_c\tau)^2/l^2] d\tau. \quad (10)$$

Integration of expression 10 is performed analytically,

$$\frac{\pi^{1/2} \exp\left[\frac{-4\xi^2 + 4i\tau_s^2 u_c \xi \omega - l_s^2 \tau_s^2 \omega^2}{4(l_s^2 + \tau_s^2 u_c^2)}\right]}{\sqrt{1/\tau_s^2 + u_c^2/l_s^2}}. \quad (11)$$

Expression 11 is used with Eqn. 3,

$$\begin{aligned} S(\mathbf{x}, \omega) &= \rho_{\infty}^2 c_{\infty}^4 \int_{-\infty}^{\infty} \dots \int_{-\infty}^{\infty} \sum_{n=1}^3 \sum_{m=1}^3 \pi_g^{n*}(\mathbf{x}, \mathbf{y}, \omega) \pi_g^m(\mathbf{x}, \mathbf{y} + \boldsymbol{\eta}, \omega) \\ &\times \frac{a_{mn} K(\mathbf{y}) p_s(\mathbf{y}) p_s(\mathbf{y} + \boldsymbol{\eta})}{\rho^2 c^2 l^2} \frac{\pi^{1/2} \exp\left[\frac{-4\xi^2 + 4i\tau_s^2 u_c \xi \omega - l_s^2 \tau_s^2 \omega^2}{4(l_s^2 + \tau_s^2 u_c^2)}\right]}{\sqrt{1/\tau_s^2 + u_c^2/l_s^2}} \\ &\times \exp[-(\eta^2 + \zeta^2)/l_{\perp}^2] d\boldsymbol{\eta} d\mathbf{y}. \end{aligned} \quad (12)$$

Over the distance where the spatial correlation is significant we assume that,

$$\pi_g^m(\mathbf{x}, \mathbf{y} + \boldsymbol{\eta}, \omega) = \pi_g^m(\mathbf{x}, \mathbf{y}, \omega) \exp\left[i \frac{\omega}{c_{\infty}} \frac{\mathbf{x}}{|\mathbf{x}|} \cdot \boldsymbol{\eta}\right], \quad (13)$$

as shown by Tam and Auriault [25]. We now examine the term $p_s(\mathbf{y} + \boldsymbol{\eta})$ shown in Eqn. 12. Morris and Miller [6] noted that the variation of the Fourier transform of the shock pressure can be written as,

$$p_s(k_1, y_2, y_3) = \int_{-\infty}^{\infty} p_s(\mathbf{y}) \exp[ik_1 y_1] dy_1, \quad (14)$$

where \mathbf{k} is the spatial wavenumber. It is observed that the variation of $p_s(k_1, \eta, \zeta)$ changes little across the jet core and shear layer where the BB-SAN source is located and is certainly a valid approximation as long as the

variation is small within regions of slowly varying shock pressure. Likewise, the same argument applies in the untransformed domain in conjunction with the observation that the spreading rate of the jet is small and that the shock cell interactions generally occur at the same radius. With these assumptions it is argued,

$$p_s(\mathbf{y} + \boldsymbol{\eta}) \simeq p_s(\mathbf{y} + \boldsymbol{\xi}). \quad (15)$$

We choose to use Eqn. 15 as it makes the analysis for scaling much simpler. Substituting Eqns. 13 and 15 into Eqn. 12 and isolating the terms of η and ζ yields an expression of the integrals involving η and ζ ,

$$\int_{-\infty}^{\infty} \int_{-\infty}^{\infty} \exp \left[\frac{-i\omega x_2 \eta}{c_{\infty} |\mathbf{x}|} \right] \exp \left[\frac{-i\omega x_3 \zeta}{c_{\infty} |\mathbf{x}|} \right] \exp \left[\frac{-(\eta^2 + \zeta^2)^2}{l_{\perp}^2} \right] d\eta d\zeta. \quad (16)$$

The integrals are evaluated analytically,

$$\pi l_{\perp}^2 \exp \left[\frac{-l_{\perp}^2 (x_2^2 + x_3^2) \omega^2}{4c_{\infty}^2 |\mathbf{x}|^2} \right]. \quad (17)$$

Expression 17 is now used to simplify Eqn. 12. Let us now restrict our model to the sideline direction, $\theta = \pi/2$. At the sideline direction π_g^2 is dominant relative to the other components,

$$\begin{aligned} S_{\theta=\pi/2}(\omega) &= \pi^{3/2} \rho_{\infty}^2 c_{\infty}^4 \int_{-\infty}^{\infty} \dots \int_{-\infty}^{\infty} \pi_g^{2*}(\mathbf{x}, \mathbf{y}, \omega) \pi_g^2(\mathbf{x}, \mathbf{y}, \omega) \\ &\exp \left[\frac{i\omega x_1 \xi}{c_{\infty} |\mathbf{x}|} \right] \frac{p_s(\mathbf{y}) p_s(\mathbf{y} + \boldsymbol{\xi})}{\rho^2 c^2 l^2} a_{22} K(\mathbf{y}) \frac{\exp \left[\frac{-4\xi^2 - 4i\tau_s^2 u_c \xi \omega - l_s^2 \tau_s^2 \omega^2}{4(l_s^2 + \tau_s^2 u_c^2)} \right]}{\sqrt{1/\tau_s^2 + u_c^2/l_s^2}} \\ &\quad \times l_{\perp}^2 \exp \left[\frac{-l_{\perp}^2 \omega^2}{4c_{\infty}^2} \right] d\xi d\mathbf{y}. \end{aligned} \quad (18)$$

The sources of BBSAN are at relatively discrete locations which is unlike mixing noise. The integrals of Eqn. 18 are replaced with summations of the integrand over the source regions,

$$\begin{aligned}
S_{\theta=\pi/2}(\omega) &= \pi^{3/2} \rho_\infty^2 c_\infty^4 \sum_{a=1}^A \sum_{b=1}^A \pi_g^{2*}(\mathbf{x}, \mathbf{y}, \omega) \pi_g^2(\mathbf{x}, \mathbf{y}, \omega) \\
&\times \exp \left[\frac{i\omega x_1 \xi}{c_\infty |\mathbf{x}|} \right] \frac{p_s(\mathbf{y}) p_s(\mathbf{y} + \xi)}{\rho^2 c^2 l^2} a_{22} K(\mathbf{y}) \frac{\exp \left[\frac{-4\xi^2 - 4i\tau_s^2 u_c \xi \omega - l_s^2 \tau_s^2 \omega^2}{4(l_s^2 + \tau_s^2 u_c^2)} \right]}{\sqrt{1/\tau_s^2 + u_c^2/l_s^2}} \\
&\times l_\perp^2 \exp \left[\frac{-l_\perp^2 \omega^2}{4c_\infty^2} \right] \underline{V}_a.
\end{aligned} \tag{19}$$

where \underline{V}_a is the local source volume and distance ξ around each shock wave – shear layer interaction, a and b . The total number of shock wave – shear layer interactions is A . a_{22} is an element of the a_{mn} tensor. If we restrict our analysis to the contribution from a single shock wave – shear layer interaction then $\xi = 0$ and Eqn. 19 becomes,

$$\begin{aligned}
S_{\theta=\pi/2}(\omega) &= \underbrace{\pi^{3/2} \rho_\infty^2 c_\infty^4}_{\text{prefactor}} \underbrace{\pi_g^{2*} \pi_g^2}_{\text{propagation}} \exp \left[\frac{-l_s^2 \tau_s^2 \omega^2}{4(l_s^2 + \tau_s^2 u_c^2)} \right] \exp \left[\frac{-l_\perp^2 \omega^2}{4c_\infty^2} \right] \\
&\times \underbrace{\frac{a_{22} p_s^2 l_\perp^2 K}{\rho^2 c^2 l^2 \sqrt{1/\tau_s^2 + u_c^2/l_s^2}}}_{\text{source}} \underline{V},
\end{aligned} \tag{20}$$

where \underline{V} is the local source volume. The first term, ‘prefactor,’ has no effect on the scaling of BBSAN while varying TTR. The second term, ‘propagation,’ is the vector Green’s function components. It quantifies the effect of the sound propagation of BBSAN and is important for capturing temperature effects. The third labeled term, ‘source,’ results from the choice of the equivalent source. The turbulent kinetic energy, K , and the local properties of ρ , c , and the integral scales of turbulence at the shock wave – shear layer interaction control the scaling in the ‘source’ term. The two exponential terms of Eqn. 20, based on numerical variation relative to the ‘source’ term, have little effect on the variation of the spectral density with increasing temperature. However, the exponential terms are included in the predictions in the following section for accuracy and completeness.

Morris and Boluriaan [31] have shown that $|\pi_g^2(\mathbf{x}, \mathbf{y}; \omega)|^2 = \omega^2 / (16\pi^2 c_\infty^6 x^2)$ for the far-field at the sideline angle for axisymmetric jets. Here it results in,

$$\begin{aligned}
S_{\theta=\pi/2}(\omega) &= \frac{\rho_\infty^2 a_{22} K p_s^2 \omega^2}{16\pi^{1/2} c_\infty^2 x^2 \rho^2 c^2 \sqrt{1/\tau_s^2 + u_c^2/l_s^2}} \\
&\times \exp\left[\frac{-l_s^2 \tau_s^2 \omega^2}{4(l_s^2 + \tau_s^2 u_c^2)}\right] \exp\left[\frac{-l_\perp^2 \omega^2}{4c_\infty^2}\right] V.
\end{aligned} \tag{21}$$

Equations 20 and 21 yield the BBSAN intensity from a single shock wave – shear layer interaction in the sideline direction. In the following sections we will evaluate Equation 19 for the acoustic intensity from BBSAN at the peak frequencies in the sideline direction for multiple jet conditions for all source interactions.

3 Results

Four cases are selected to exercise Eqn. 19. The cases represent over-expanded and under-expanded conditions over a range of Mach numbers for a convergent and convergent-divergent nozzle. The nozzles and operating conditions are shown in table 1 and the TTR varies from 1.00 to 4.00 for each case. The first row of the table shows the conditions of the convergent nozzle and has corresponding data collected from the small hot jet acoustic rig (SHJAR) experiment of Bridges and Brown [8]. The remaining three rows of the table correspond to three of the four conditions performed in the experiment of Kuo *et al.* [7].

A CFD calculation is performed for each experimental condition summarized in table 1. The arguments of the acoustic analogy are related to the steady RANS solution. The equivalent sources could easily be informed by a more advanced simulation that uses LES or simpler empirical models.

3.1 Steady Reynolds-Averaged Navier-Stokes Solutions

The Wind-US CFD (see Nelson [32] for details) solver is used to calculate the steady RANS solutions. Calculations are performed from TTR = 1.00 to 4.00 in increments of 0.1 for TTR = 1.00 to 2.50 and increments of 0.25 from TTR = 2.50 to 4.00. All simulations are axisymmetric and are closed by the Menter [33] Shear Stress Transport (SST) turbulence model. Details for these types of simulations and experimental validation of the flow-fields have been discussed by Miller and Veltin [34].

M_d	D (m)	M_j	NPR	Origin	Type
1.00	0.0508	1.50	3.67	Bridges and Brown	Convergent
1.50	0.0127	1.20	2.42	Kuo <i>et al.</i>	Convergent-Divergent
1.50	0.0127	1.70	4.94	Kuo <i>et al.</i>	Convergent-Divergent
1.50	0.0127	1.90	6.70	Kuo <i>et al.</i>	Convergent-Divergent

Table 1: Properties of the jet flows. For each row a simulation is performed at TTR 1.00 to 2.50 at increments of 0.10 and from TTR 2.50 to 4.00 in increments of 0.25. In total 80 steady RANS solutions are performed.

By examining table 1, it can be shown that only four NPR are required and only four unique values of β result. Changing TTR while holding the NPR constant results in nearly identical shock-cell structures. Contours of p/p_∞ are shown in Fig. 3 where the axes are normalized by the jet diameter. Steady RANS solutions are mirrored about the x -axis for illustration purposes. The jet conditions in Fig. 3 are a) $M_d = 1.50$, $M_j = 1.20$, TTR = 1.00, $D = 0.0127$ m, b) $M_d = 1.00$, $M_j = 1.50$, TTR = 1.00, $D = 0.0508$ m, c) $M_d = 1.50$, $M_j = 1.70$, TTR = 1.00, $D = 0.0127$ m, and d) $M_d = 1.50$, $M_j = 1.90$, $D = 0.0127$ m, TTR = 1.00. The circles in parts a) through d) represent the time averaged locations where conical oblique shock waves interact with the jet shear layer. The shock cell shear layer interactions represent the positions where BBSAN sources are located. At each shock wave – shear layer interaction, the field variables are extracted as a function of TTR from the steady RANS solutions.

To illustrate the relative source strength and location of the BBSAN sources, a numerical investigation is performed with a $M_d = 1.00$, $M_j = 1.50$, TTR = 1.00, and $D = 0.0254$ m jet. A steady RANS solution of this flow-field is shown in Fig. 4. Part a) shows contours of shock pressure and part b) shows contours of turbulent kinetic energy. Part c) shows contours of the integrand of the model of Morris and Miller [6] at $\psi = 90$ degrees and $R/D = 100$. The contours of part c) represent the relative strength of BBSAN at the peak BBSAN frequency. At this source location the high values of p_s and K can be observed in part a) and b) respectively and indeed, as theory suggests, correspond to shock wave – shear layer interactions. Measurements, such as those of Norum and Seiner [35], show that the BBSAN source is further downstream than predicted. However, in their study there is no account for the refraction effects of the jet shear layer. In supersonic jets, refraction

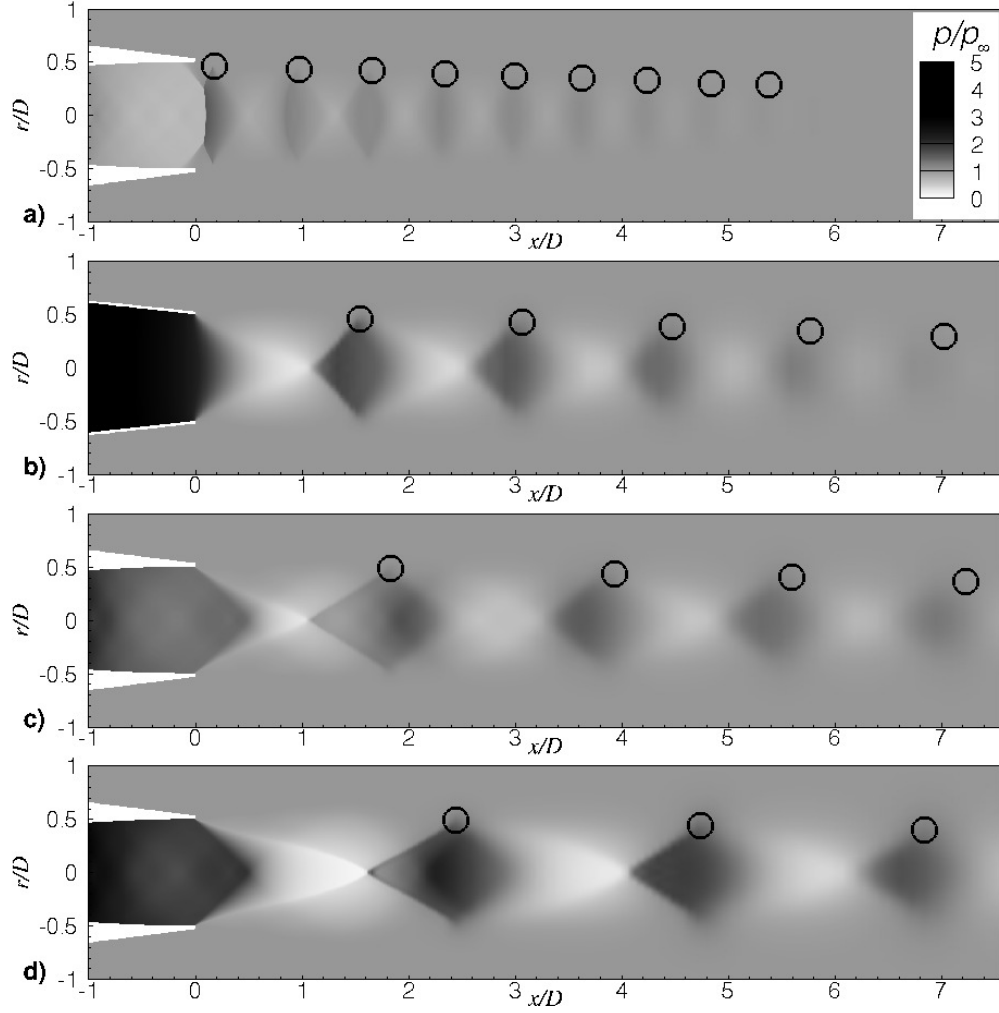


Figure 3: Contours of pressure p/p_∞ of the four jet families studied. The circles represent locations of the oblique shock wave – shear layer interactions. Flow-field data is extracted as a function of TTR at these locations. The jet conditions shown are, a) $M_d = 1.50$, $M_j = 1.20$, TTR = 1.00, b) $M_d = 1.00$, $M_j = 1.50$, TTR = 1.00, c) $M_d = 1.50$, $M_j = 1.70$, TTR = 1.00, and d) $M_d = 1.50$, $M_j = 1.90$, TTR = 1.00.

effects can make sources appear multiple diameters downstream from their actual location.

3.2 Scaling of Broadband Shock-Associated Noise with Temperature

A comparison of the predicted source scaling of the BBSAN with measurement is shown in Fig. 5 for the convergent nozzle, $M_j = 1.50$, and varying TTR. The contribution predicted by Eqn. 19 is shown as a black line with round circles. The dashed line with triangles is the prediction of Morris and Miller [6] without the use of the empirical correction factor, T_{cf} . The data from the SHJAR experiment is shown as red squares. Experimental values represent the maximum BBSAN at the sideline location of the jet. The evaluation of the intensity has been performed based on the locations shown in Fig. 3 part b). The factor T_{cf} is not included in the predictions using Eqn. 19 or those derived from Morris and Miller [6]. It is clear that with increasing TTR the prediction of Eqn. 19 initially increases linearly with TTR and eventually saturates.

The following comparisons are performed with the experiment of Kuo *et al.* [7] who used a $M_d = 1.50$, $D = 0.0127$ m nozzle, and varied the TTR. Figure 6 shows comparisons at $R/D = 100$ and at the sideline location with $M_j = 1.20$. These particular jet conditions produced no screech tones through their entire temperature range. The scaling of the source shows a clear increase from TTR = 1.00 and saturates at relatively the same rate as the experiment.

For the next comparison, the same nozzle and observer location is retained but the jet operates at $M_j = 1.70$. Comparisons between the predicted peak BBSAN and Kuo *et al.* [7] are shown in Fig. 7. Unlike the previous case, these jet conditions produced very strong screech tones. The over-pressure of the screech, S_o , is marked at each data point in the figure. S_o is a measure of the maximum screech amplitude minus the broadband level at the fundamental screech frequency. The screech frequency is often lower than the peak BBSAN frequency. To illustrate this point, reexamine Fig. 1 at the sideline location, where the fundamental screech tone frequency is lower than the peak BBSAN frequencies. The tone labeled screech is the fundamental screech tone and its overpressure is approximately 12 dB. In Fig. 7 the maximum BBSAN has corresponding values of S_o that change with TTR. At low temperatures

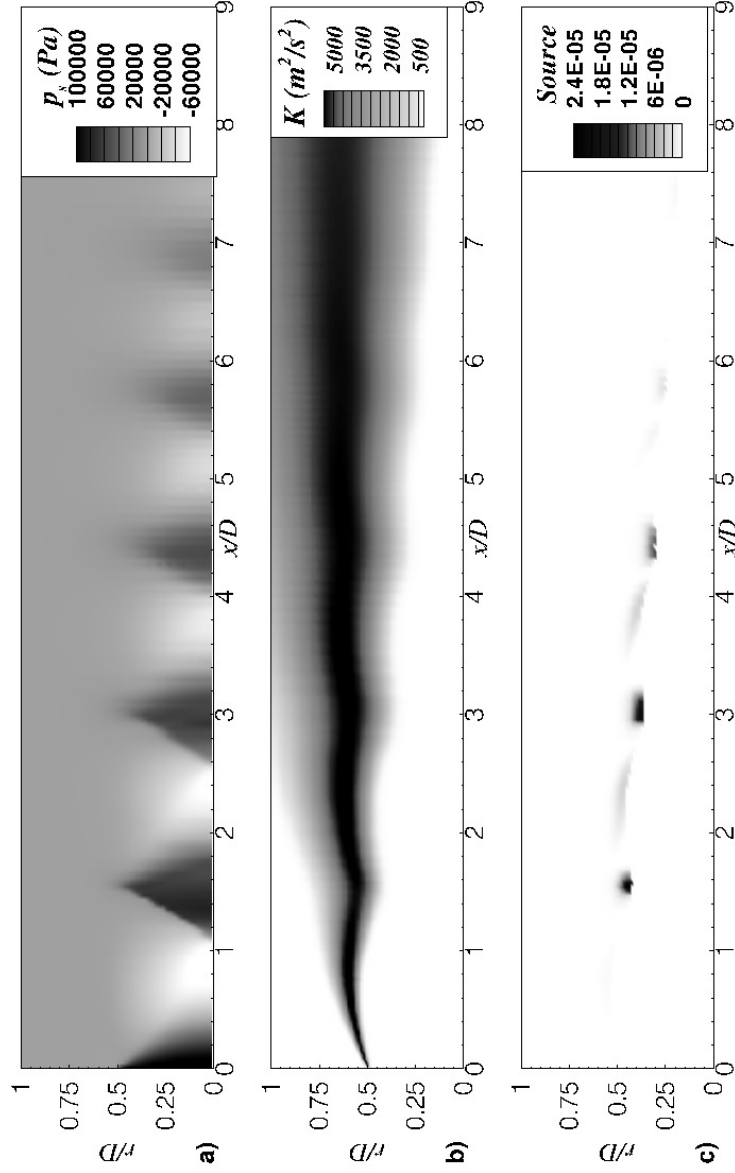


Figure 4: A $M_d = 1.00$, $M_j = 1.50$, TTR = 1.00, $D = 0.0254$ m jet produces contours of, a) shock pressure, b) turbulent kinetic energy, K , c) integrand of the model of Morris and Miller [6] at the sideline location at $R/D = 100$ and peak BBSAN frequency (contours of BBSAN source strength). Note in c), the maximum BBSAN source occurs at the location where the shock wave – shear layer interactions occur.

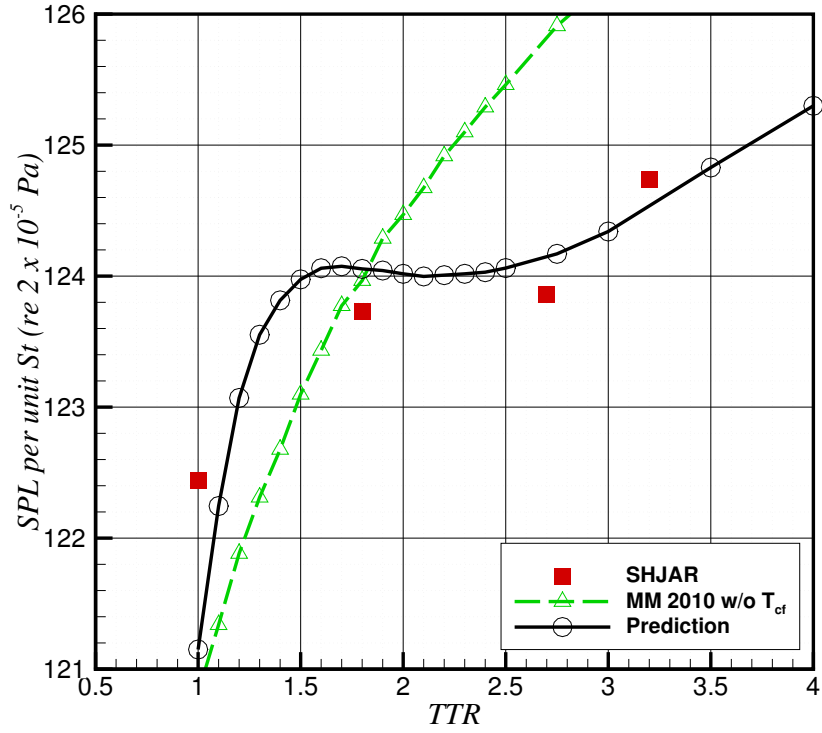


Figure 5: Variation of maximum BBSAN intensity from a $M_d = 1$, $M_j = 1.5$ (experiment performed at $M_j = 1.469$) jet relative to increasing TTR. The observer is located at $R/D = 100$ and $\psi = 90$ degrees. The prediction of Eqn. 19 is compared with measurement of the maximum BBSAN.

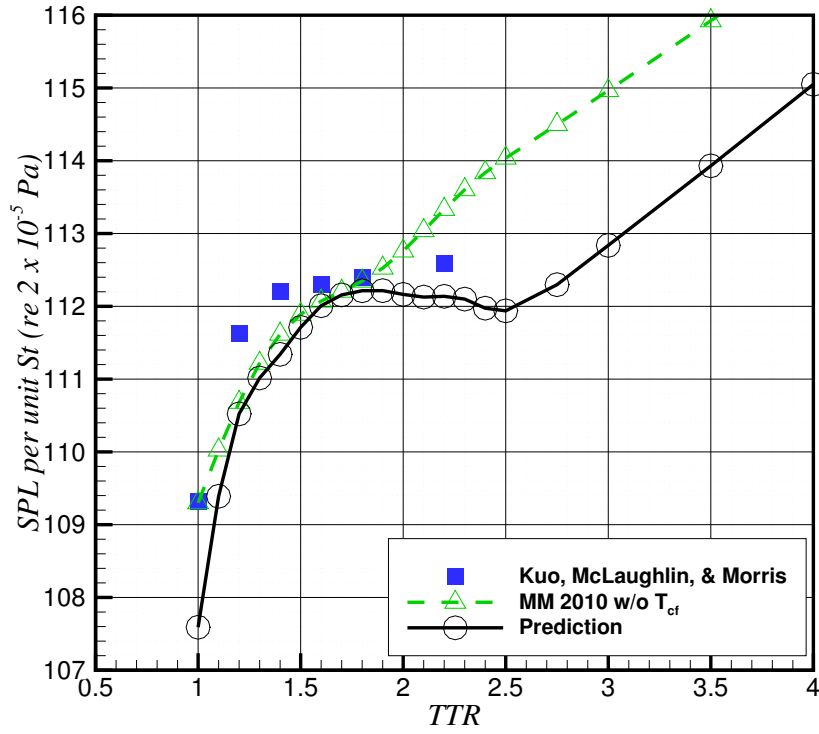


Figure 6: Variation of maximum BBSAN intensity from a $M_d = 1.5$, $M_j = 1.2$ jet relative to increasing TTR. The observer is located at $R/D = 100$ and $\psi = 90$ degrees. The prediction of Eqn. 19 is compared with measurement of the maximum BBSAN.

the screech over-pressure is large and as the TTR increases the screech over-pressure approaches zero. In Fig. 5 where S_o is relatively constant and non-zero and Fig. 6 where there is no screech, the agreement between prediction and experiment is arguably better. If the screech over-pressure is constant through the range of TTR or preferably, zero, as it is typically in full-scale engines, then the effects of screech on the BBSAN are relatively the same and the scaling of BBSAN is accurately captured. In Fig. 7, one may observe the correct trend of BBSAN saturation starting at $TTR = 1.4$. The BBSAN is amplified a large amount due to the large screech amplitudes present at low temperatures.

A final comparison is made between the prediction of the scaling using Eqn. 19 and the experiment of Kuo *et al.* [7] in Fig. 8. The fully expanded Mach number is increased to 1.90 and all other conditions are retained. The similarity between the prediction of Eqn. 19 and measurement of Kuo *et al.* [7] at moderate to higher TTR is similar to that of Fig. 7. At low temperatures the screech tones have disrupted the trend due to reasons previously described, and the correct scaling of BBSAN is not captured. If screech were not present within the experiments then the trends at low TTR for Figs. 7 and 8 will yield a lowered BBSAN amplitude, and eventual saturation as seen in Figs. 5 and 6 will occur.

It is evident that the inclusion of using local properties for the streamwise velocity component and density (in the denominator of the source term), instead of ambient quantities, and the combination of the vector Green's function that is amplified by the shear layer, yields a model that is more consistent with experiment.

Unheated and slightly heated jets are difficult to predict due to the rapid variation of BBSAN intensity. Not only are the predictions very difficult to conduct both mathematically and in terms of implementation but the experiments are very difficult to perform. Note the nozzle diameter is on the order of 10^{-2} m. The difficulty of acquiring high quality experimental data cannot be overstated.

Screech tones are extremely sensitive to laboratory conditions and are highly nonlinear. However, all fluid dynamic phenomena are deterministic. When the screech over-pressure is very high at low TTR, the BBSAN is lowered in frequency and raised in amplitude. It could be possible for an experiment to be performed for the same jet conditions as shown in this paper, but without screech and without screech's effect on the mixing noise or BBSAN. It is expected that the peak BBSAN intensity levels, without the

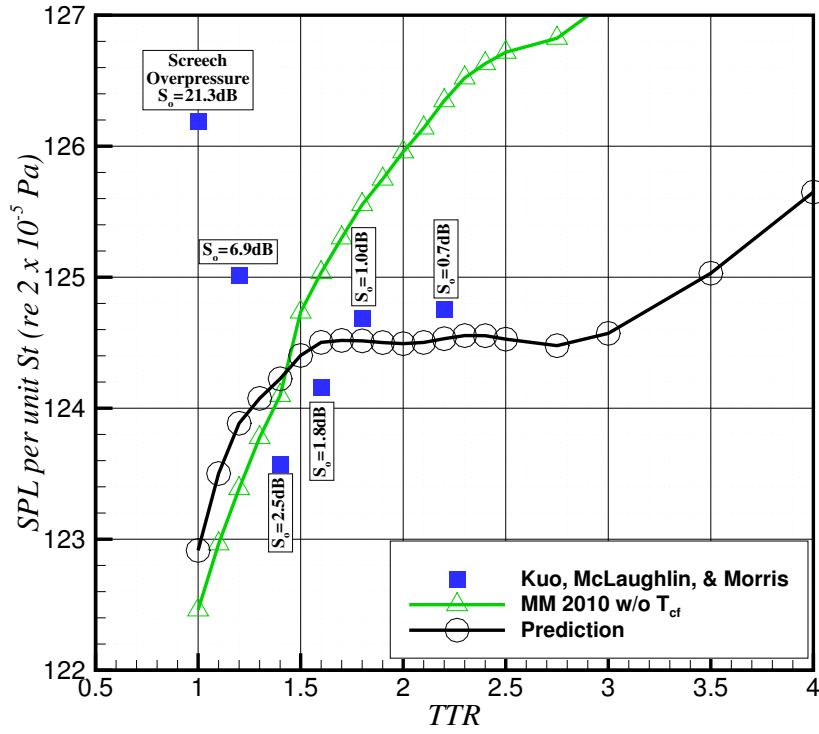


Figure 7: Variation of maximum BBSAN intensity from a $M_d = 1.5$, $M_j = 1.7$ jet relative to increasing TTR. The observer is located at $R/D = 100$ and $\psi = 90$ degrees. The prediction of Eqn. 19 is compared with measurement of the maximum BBSAN.

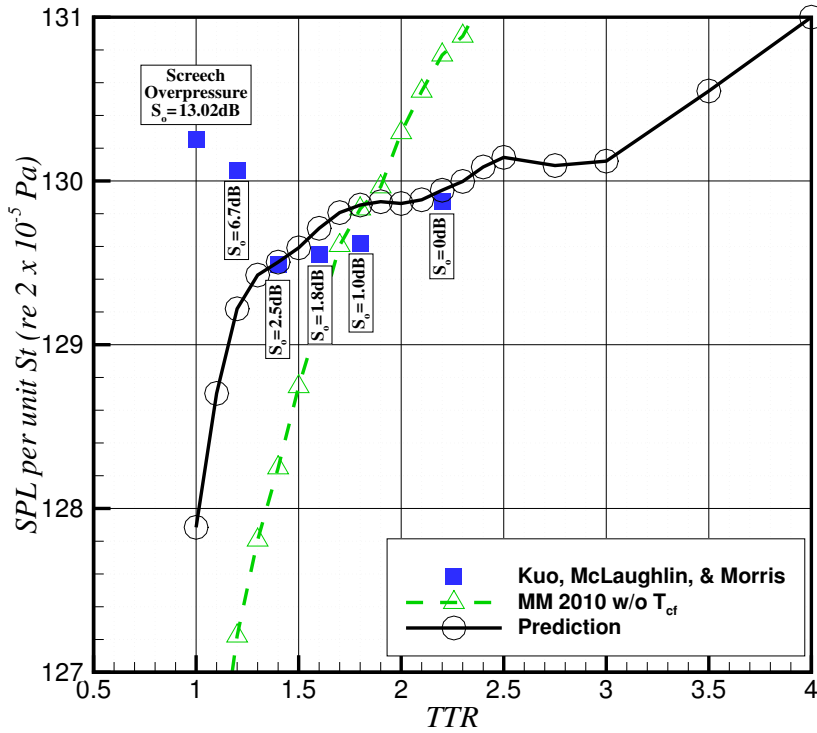


Figure 8: Variation of maximum BBSAN intensity from a $M_d = 1.5$, $M_j = 1.9$ jet relative to increasing TTR. The observer is located at $R/D = 100$ and $\psi = 90$ degrees. The prediction of Eqn. 19 is compared with measurement of the maximum BBSAN.

influence of the discrete tone, will compare with the developed theory.

4 Conclusion

BBSAN intensity saturates with increasing jet stagnation temperature. This saturation occurs due to the balance between the source term and the propagation effects. An equivalent source for BBSAN is proposed that takes into account the scaling of both NPR and TTR. The scaling term is contained within the developed acoustic analogy and contains the effects of the equivalent source and propagation separately. This acoustic analogy is evaluated with arguments corresponding to four families of disintegrated jets. Evaluation involves extracting the local properties at the shock wave – shear layer interactions from steady RANS solutions. These local field variables are arguments of the source term. Comparisons of the predicted peak BBSAN intensity from shock wave – shear layer interactions show the same trend as measurement. The predictions, like the experiments, show eventual saturation with increasing jet stagnation temperature. At very high temperature ratios predictions show that saturation ceases and the BBSAN intensity will again rise. Higher fidelity measurements, without screech, are required to further validate this theory.

Acknowledgements

The author benefited greatly from discussions with Boeing/A. D. Welliver Professor Philip J. Morris of the Pennsylvania State University. The availability of experimental data from Professor Dennis K. McLaughlin of the Pennsylvania State University, Dr. James Bridges of NASA Glenn Research Center at Lewis Field, and Dr. Viswanathan of the Boeing Company made this work possible. The author is grateful for continuous support from The National Aeronautics and Space Administration Fundamental Aeronautics Program High Speed Project.

References

- [1] Farassat, F., “The Sound from Rigid Bodies in Arbitrary Motion,” Cornell University Ph.D. Dissertation, January 1973.
- [2] Ffowcs Williams, J. E. and Hawkings, D. L., “Sound Generation by Turbulence and Surfaces in Arbitrary Motion,” *Phil. Trans. R. Soc. Lond. A*, Vol. 264, No. 1151, 1969, pp. 321–342. doi:[10.1098/rsta.1969.0031](https://doi.org/10.1098/rsta.1969.0031).
- [3] Farassat, F., “Linear Acoustic Formulas for Calculation of Rotating Blade Noise,” *AIAA Journal*, Vol. 19, No. 9, 1981, pp. 1122–1130. doi:[10.2514/3.60051](https://doi.org/10.2514/3.60051).
- [4] Farassat, F. and Succi, G. P., “A Review of Propeller Discrete Frequency Noise Prediction Technology with Emphasis on Two Current Methods for Time Domain Calculations,” *Journal of Sound and Vibration*, Vol. 71, No. 3, 1980, pp. 399–419. doi:[10.1016/0022-460X\(80\)90422-8](https://doi.org/10.1016/0022-460X(80)90422-8).
- [5] Farassat, F. and Myers, M. K., “Multidimensional Generalized Functions in Aeroacoustics and Fluid Mechanics-Part 1: Basic Concepts and Operations,” *International Journal of Aeroacoustics*, Vol. 10, No. 2-3, June 2011, pp. 161–200. doi:[10.1260/1475-472X.10.2-3.161](https://doi.org/10.1260/1475-472X.10.2-3.161).
- [6] Morris, P. J. and Miller, S. A. E., “Prediction of Broadband Shock-Associated Noise Using Reynolds-Averaged Navier-Stokes Computational Fluid Dynamics,” *AIAA Journal*, Vol. 48, No. 12, 2010, pp. 2931–2961. doi:[10.2514/1.J050560](https://doi.org/10.2514/1.J050560).
- [7] Kuo, C., McLaughlin, D. K., and Morris, P. J., “Effects of Supersonic Jet Conditions on Broadband Shock-Associated Noise,” *49th AIAA Aerospace Sciences Meeting, AIAA Paper 2011-1032*, 2011. doi:[10.2514/6.2011-1032](https://doi.org/10.2514/6.2011-1032).
- [8] Bridges, J. and Brown, C. A., “Validation of the Small Hot Jet Acoustic Rig for Aeroacoustic Research,” *11th AIAA/CEAS Aeroacoustics Conference, May 23-25, AIAA Paper 2005-2846*, 2005. doi:[10.2514/6.2005-2846](https://doi.org/10.2514/6.2005-2846).
- [9] Powell, A., “On the Noise Emanating from a Two-Dimensional Jet above the Critical Pressure,” *Aeronautical Quarterly*, Vol. 4, 1953, pp. 103–122.

- [10] Harper-Bourne, M. and Fisher, M. J., “The Noise from Shock-Waves in Supersonic Jets,” AGARD Conference Proceedings, 1973.
- [11] Raman, G., “Supersonic Jet Screech: Half-Century from Powell to the Present,” *Journal of Sound and Vibration*, Vol. 225, No. 3, 1999, pp. 543–571. doi:[10.1006/jsvi.1999.2181](https://doi.org/10.1006/jsvi.1999.2181).
- [12] Ffowcs Williams, J. E., “Hydrodynamic Noise,” *Annual Review of Fluid Mechanics*, Vol. 1, 1969, pp. 197–222. doi:[10.1146/annurev.fl.01.010169.001213](https://doi.org/10.1146/annurev.fl.01.010169.001213).
- [13] Ffowcs Williams, J. E., “Aeroacoustics,” *Annual Review of Fluid Mechanics*, Vol. 9, 1977, pp. 447–68. doi:[10.1146/annurev.fl.09.010177.002311](https://doi.org/10.1146/annurev.fl.09.010177.002311).
- [14] Goldstein, M. E., “Aeroacoustics of Turbulent Shear Flows,” *Annual Review of Fluid Mechanics*, Vol. 16, 1984, pp. 263–285. doi:[10.1146/annurev.fl.16.010184.001403](https://doi.org/10.1146/annurev.fl.16.010184.001403).
- [15] Tam, C. K. W., “Supersonic Jet Noise,” *Annual Review of Fluid Mechanics*, Vol. 27, 1995, pp. 17–43. doi:[10.1146/annurev.fl.27.010195.000313](https://doi.org/10.1146/annurev.fl.27.010195.000313).
- [16] Viswanathan, K., Alkisar, M. B., and Czech, M. J., “Characteristics of the Shock Noise Component of Jet Noise,” *AIAA Journal*, Vol. 48, No. 1, 2010, pp. 25–46. doi:[10.2514/1.38521](https://doi.org/10.2514/1.38521).
- [17] Andre, B., Castelain, T., and Bailly, C., “Broadband Shock-Associated Noise in Screeching and Non-Screeching Underexpanded Supersonic Jets,” *AIAA Journal*, Vol. 51, No. 3, March 2013, pp. 665–673. doi:[10.2514/1.J052058](https://doi.org/10.2514/1.J052058).
- [18] Tam, C. K. W., “Stochastic Model Theory of Broadband Shock-Associated Noise from Supersonic Jets,” *Journal of Sound and Vibration*, Vol. 116, No. 2, 1987, pp. 265–302. doi:[10.1016/S0022-460X\(87\)81303-2](https://doi.org/10.1016/S0022-460X(87)81303-2).
- [19] Tam, C. K. W. and Tanna, H. K., “Shock-Associated Noise of Supersonic Jets from Convergent-Divergent Nozzles,” *Journal of Sound and Vibration*, Vol. 81, No. 3, 1982, pp. 337–358. doi:[10.1016/0022-460X\(82\)90244-9](https://doi.org/10.1016/0022-460X(82)90244-9).

- [20] Pack, D. C., “A Note on Prandtl’s Formula for the Wavelength of a Supersonic Gas Jet,” *Quarterly Journal of Applied Mathematics and Mechanics*, Vol. 3, 1950, pp. 173–181.
- [21] Tam, C. K. W. and Chen, K. C., “A Statistical Model of Turbulence in Two-Dimensional Mixing Layers,” *Journal of Fluid Mechanics*, Vol. 92, 1979, pp. 303–326. doi:[10.1017/S002211207900063X](https://doi.org/10.1017/S002211207900063X).
- [22] Tam, C. K. W., “Broadband Shock-Associated Noise of Moderately Imperfectly-Expanded Supersonic Jets,” *Journal of Sound and Vibration*, Vol. 140, No. 1, 1990, pp. 55–71. doi:[10.1016/0022-460X\(90\)90906-G](https://doi.org/10.1016/0022-460X(90)90906-G).
- [23] Doty, M. J. and McLaughlin, D., “Acoustic and Mean Flow Measurements of High-Speed Helium-Air Mixture Jets,” *International Journal of Aeroacoustics*, Vol. 2, No. 2, 2003, pp. 293–334. doi:[10.1260/147547203322986151](https://doi.org/10.1260/147547203322986151).
- [24] Lilley, G. M., “On the Noise from Jets,” *AGARD Conference Proceedings In Noise Mechanisms*, Vol. 13, 1974, pp. 1–11.
- [25] Tam, C. K. W. and Auriault, L., “Mean Flow Refraction Effects on Sound Radiated from Localized Sources in a Jet,” *Journal of Fluid Mechanics*, Vol. 370, 1998, pp. 149–174. doi:[10.1017/S0022112098001852](https://doi.org/10.1017/S0022112098001852).
- [26] Raizada, N., “Numerical Prediction of Noise from High Speed Subsonic Jets using an Acoustic Analogy,” *Ph.D. Dissertation, The Pennsylvania State University*, December 2005.
- [27] Khavaran, A., Bridges, J., and Georgiadis, N., “Prediction of Turbulence-Generated Noise in Unheated Jets,” *NASA TM-2005-213827*, 2005.
- [28] Miller, S. A. E. and Morris, P. J., “The Prediction of Broadband Shock-Associated Noise Including Propagation Effects,” *International Journal of Aeroacoustics*, Vol. 11, No. 8, 2012, pp. 755–782. doi:[10.1260/1475-472X.11.7-8.755](https://doi.org/10.1260/1475-472X.11.7-8.755).
- [29] Henry, C., Bailly, C., and Bodard, G., “Statistical Modeling of BBSAN Including Refraction Effects,” *AIAA Aeroacoustics Conference, AIAA Paper 2012-2163*, 2012. doi:[10.2514/6.2012-2163](https://doi.org/10.2514/6.2012-2163).

- [30] Ribner, H. S., “The Generation of Sound by Turbulent Jets,” *Advances in Applied Mechanics*, Vol. 8, 1964, pp. 103–182. doi:[10.1016/S0065-2156\(08\)70354-5](https://doi.org/10.1016/S0065-2156(08)70354-5).
- [31] Morris, P. J. and Boluriaan, S., “The Prediction of Jet Noise from CFD Data,” *10th AIAA/CEAS Aeroacoustics Conference, AIAA Paper 2004-2977*, 2004. doi:[10.2514/6.2004-2977](https://doi.org/10.2514/6.2004-2977).
- [32] Nelson, C., “An Overview of the NPARC Alliance’s Wind-US Flow Solver,” *48th AIAA Aerospace Sciences Meeting, AIAA Paper 2010-27*, 2010. doi:[10.2514/6.2010-27](https://doi.org/10.2514/6.2010-27).
- [33] Menter, F. R., “Two-Equation Eddy-Viscosity Turbulence Models for Engineering Applications,” *AIAA Journal*, Vol. 32, No. 8, 1994, pp. 1598–1605. doi:[10.2514/3.12149](https://doi.org/10.2514/3.12149).
- [34] Miller, S. A. E. and Veltin, J., “Assessment of Computational Fluid Dynamics for Supersonic Shock Containing Jets,” *AIAA Journal*, Vol. 47, No. 11, 2009, pp. 2738–2746. doi:[10.2514/1.44336](https://doi.org/10.2514/1.44336).
- [35] Norum, T. D. and Seiner, J. M., “Broadband Shock Noise from Supersonic Jets,” *AIAA Journal*, Vol. 20, No. 1, 1982, pp. 68–73. doi:[10.2514/3.51048](https://doi.org/10.2514/3.51048).